Higher order beam finite elements with only displacement degrees of freedom

Erasmo Carrera[1], Marco Petrolo[1], Christian Wenzel[1], Gaetano Giunta[1,2], Salim Belouettar[2]
[1]*Aeronautics and Space Engineering Department, Politecnico di Torino, Italy*
[2] *Centre de Recherche Public Henri Tudor, Luxembourg*
E-mail: erasmo.carrera@polito.it, marco.petrolo@polito.it, christian.wenzel@studenti.polito.it, gaetano.giunta@polito.it, Salim.belouettar@tudor.lu

Keywords: Refined finite elements, Carrera Unified Formulation, higher-order theories.

SUMMARY. This paper presents higher order beam elements with only displacement degrees of freedom based on Carrera Unified Formulation (CUF). The displacement components are expanded in terms of cross-section coordinates, (x, y), by using N-order Lagrange polynomials which are defined on a set of sampling points. The displacements of these points are the variables of the structural problem. CUF hierarchical implementation offers the capability of considering N as a free parameter of the formulation. Refined models are obtained either by increasing N, or by opportunely assembling multiple Lagrange elements on the cross-section. Linear, quadratic and cubic approximations along the beam axis, (z), are introduced to develop finite element matrices. These are obtained in terms of a few fundamental nuclei whose form is independent by both N and the number of element nodes. Convergence and assessments with available results is first made. Additional analyses consider free vibrations responses. It is mainly concluded that refined beam models based on Lagrange polynomials furnish reliable and accurate results. Their use offers a wide range of opportunities such as dealing with multilayered structures, detecting shell-type responses and implementing non-linear analysis.

1 INTRODUCTION

Slender bodies such us airplane wings, helicopter blades, bridges, and frames are mainly analyzed through beam theories. The use of one-dimensional 1D models is 'historically' preferred to the introduction of more cumbersome two-dimensional 2-D (plate and shell theories) and three-dimensional 3-D analyses. The proper detection of non-classical effects and shell-type responses requires the development of higher-order beam theories.
Classical 1-D models for beams made of isotropic materials are based on Euler-Bernoulli and Timoshenko theories. The former does not account for the transverse shear effects on the cross-sections deformations. The latter provides a model that foresees a constant shear deformation distribution on the cross-sections. Both of them yield better results for slender rather than short beams.
A review of several beam and plate theories for vibration, wave propagation, buckling and post-buckling was presented by Kapania and Raciti [1, 2]. Particular attention was given to models that account for transverse shear-deformation. Beside that, a review about the developments in finite element formulations for thin and thick laminated beams was provided. Kim and White [3] investigated non-classical effects in composite box beam models, such as torsional warping and transverse shear effects. They show that the larger the thickness of the wall, the more important the non-classical effects. Third-order, locking free beam element was developed by Reddy [4]. Euler-Bernoulli's and Timoshenko's models where are obtained as special cases of the proposed element. As far as free vibrations finite element analysis is concerned, higher order models are necessary to evaluate properly high number modes as highlighted by Shi and Lam [5]. Lee [6] studied the flexural-torsional

behavior of I-shaped composite beams. Transverse shear deformation, coupling and warping effects are accounted for.
Refined theories are also developed exploiting the asymptotic method [7, 8, 9], a suitable kinematics model for a structural problem is obtained by investigating the role played by the various variables in term of a perturbation parameter (usually a geometrical one such as the span-to-height ratio for beams). The 3-D problem is then reduced to a 1-D model by exploiting an asymptotic series of a characteristic parameter, and retaining those terms which exhibit the same order of magnitude when the perturbation parameter vanishes. Contributions in developing higher order beam theories by exploiting asymptotic methods can be found in [10, 11, 12].
In this paper the finite element formulation of refined beam models based on Lagrangian polynomials is addressed. Static and free vibrations analysis are conducted. Linear and quadratic approximations along the section, (x, y), are used. Convergence studies are first made. Additional analysis consider different loadings conditions (bending, traction), as well as free-vibrations analysis. Taylor-type expansions are used for validation purposes, see also [13]. In particular, Euler Bernoulli (EBBM), Timoshenko (TBM) and fourth order models are considered.

2 PRELIMINARIES

The adopted coordinate frame is presented in Figs. 1 and 2. The beam boundaries over z are $0 \leq z \leq L$. The origin is placed on the center of gravity of the section even when a generic not-rectangular shape is considered. The displacements vector is:

$$\mathbf{u}(x,y,z) = \left\{ \begin{array}{ccc} u_x & u_y & u_z \end{array} \right\}^T \tag{1}$$

Superscript T represents the transposition operator. The stress, $\boldsymbol{\sigma}$, and the strain, $\boldsymbol{\epsilon}$, are grouped as it follows:

$$\begin{array}{ll} \boldsymbol{\sigma}_p = \left\{ \begin{array}{ccc} \sigma_{xx} & \sigma_{yy} & \sigma_{xy} \end{array} \right\}^T, & \boldsymbol{\epsilon}_p = \left\{ \begin{array}{ccc} \epsilon_{xx} & \epsilon_{yy} & \epsilon_{xy} \end{array} \right\}^T \\ \boldsymbol{\sigma}_n = \left\{ \begin{array}{ccc} \sigma_{xz} & \sigma_{yz} & \sigma_{zz} \end{array} \right\}^T, & \boldsymbol{\epsilon}_n = \left\{ \begin{array}{ccc} \epsilon_{xz} & \epsilon_{yz} & \epsilon_{zz} \end{array} \right\}^T \end{array} \tag{2}$$

Subscript "n" stands for terms laying on the cross-section, while "p" stands for terms laying on planes orthogonal to Ω. In case of linear theory, the strain-displacement relations are:

$$\begin{array}{l} \boldsymbol{\epsilon}_p = \boldsymbol{D}_p \mathbf{u} \\ \boldsymbol{\epsilon}_n = \boldsymbol{D}_n \mathbf{u} = (\boldsymbol{D}_{n\Omega} + \boldsymbol{D}_{nz})\mathbf{u} \end{array} \tag{3}$$

with:

$$\boldsymbol{D}_p = \begin{bmatrix} \frac{\partial}{\partial x} & 0 & 0 \\ 0 & \frac{\partial}{\partial y} & 0 \\ \frac{\partial}{\partial y} & \frac{\partial}{\partial x} & 0 \end{bmatrix}, \quad \boldsymbol{D}_{n\Omega} = \begin{bmatrix} 0 & 0 & \frac{\partial}{\partial x} \\ 0 & 0 & \frac{\partial}{\partial y} \\ 0 & 0 & 0 \end{bmatrix}, \quad \boldsymbol{D}_{nz} = \begin{bmatrix} \frac{\partial}{\partial z} & 0 & 0 \\ 0 & \frac{\partial}{\partial z} & 0 \\ 0 & 0 & \frac{\partial}{\partial z} \end{bmatrix} \tag{4}$$

In case of orthotropic materials, Hooke law holds:

$$\boldsymbol{\sigma} = \boldsymbol{C}\boldsymbol{\epsilon} \tag{5}$$

According to Eq.s 2, the previous equation becomes:

$$\begin{array}{l} \boldsymbol{\sigma}_p = \tilde{\boldsymbol{C}}_{pp}\boldsymbol{\epsilon}_p + \tilde{\boldsymbol{C}}_{pn}\boldsymbol{\epsilon}_n \\ \boldsymbol{\sigma}_n = \tilde{\boldsymbol{C}}_{np}\boldsymbol{\epsilon}_p + \tilde{\boldsymbol{C}}_{nn}\boldsymbol{\epsilon}_n \end{array} \tag{6}$$

where matrices $\tilde{\boldsymbol{C}}_{pp}$, $\tilde{\boldsymbol{C}}_{nn}$, $\tilde{\boldsymbol{C}}_{pn}$ and $\tilde{\boldsymbol{C}}_{np}$ are:

$$\tilde{\boldsymbol{C}}_{pp} = \begin{bmatrix} \tilde{C}_{11} & \tilde{C}_{12} & \tilde{C}_{16} \\ \tilde{C}_{12} & \tilde{C}_{22} & \tilde{C}_{26} \\ \tilde{C}_{16} & \tilde{C}_{26} & \tilde{C}_{66} \end{bmatrix}, \quad \tilde{\boldsymbol{C}}_{nn} = \begin{bmatrix} \tilde{C}_{55} & \tilde{C}_{45} & 0 \\ \tilde{C}_{45} & \tilde{C}_{44} & 0 \\ 0 & 0 & \tilde{C}_{33} \end{bmatrix}, \quad \tilde{\boldsymbol{C}}_{pn} = \tilde{\boldsymbol{C}}_{np}^{T} = \begin{bmatrix} 0 & 0 & \tilde{C}_{13} \\ 0 & 0 & \tilde{C}_{23} \\ 0 & 0 & \tilde{C}_{36} \end{bmatrix} \tag{7}$$

For the sake of brevity, the dependence of the coefficients $[\tilde{C}]_{ij}$ versus Young's moduli, Poisson's ratio, the shear moduli and the fibre angle is not reported. It can be found in [14] or [15].

3 UNIFIED FORMULATION

The proposed higher-order formulation is embedded in the framework of Carrera Unified Formulation (CUF)[16]. CUF offers a systematic procedure to obtain refined structural models by considering the order of the theory, N, as a free parameter of the formulation. The displacement field is assumed as an expansion of a certain class of functions F_τ:

$$\mathbf{u} = F_\tau \mathbf{u}_\tau, \qquad \tau = 1, 2, ..., M \tag{8}$$

where F_τ are functions of the coordinates x and y on the cross-section. $\mathbf{u}_\tau$ is the displacement vector and *M* stands for the number of terms of the expansion. Linear (2 nodes, B2), quadratic (3 nodes, B3) and cubic (4 nodes, B4) shape functions, N_i, along the beam axis, (z), are introduced to develop finite element matrices. F_τ expansion can be expressed in several manners. In this work linear (Q4) and parabolic (Q9) Lagrange polynomials are exploited. For the sake of brevity, their expressions are not reported here, they can be found in [18]. The use of Lagrange expansions require the choice of a set of sampling points on the cross-sections with respect to compute the polynomials. In Figs. 3 the locations of the sampling points are shown in case of square cross-section. The variables of the problem are the displacement components of each sampling point. In case of linear expansion, the kinematics model becomes:

$$\begin{aligned} u_x &= L_1\, u_{x1} + L_2\, u_{x2} + L_3\, u_{x3} + L_4\, u_{x4} \\ u_y &= L_1\, u_{y1} + L_2\, u_{y2} + L_3\, u_{y3} + L_4\, u_{y4} \\ u_z &= L_1\, u_{z1} + L_2\, u_{z2} + L_3\, u_{z3} + L_4\, u_{z4} \end{aligned} \tag{9}$$

where $L_1, ..., L_4$ stand for the Lagrange polynomials and $u_{x1}, ..., u_{z4}$ are the displacement variables. Lagrange-type description of the cross-section kinematics offers the opportunity of stacking multiple sets of sampling points upon the cross-section. Each set has its own displacement field as well as material properties. The assembling procedure is analogue to that used with finite elements along z axis. By means of this analogy, Lagrange sets of sampling points are referred as cross-section elements. In case of two Q4 elements, the cross-section displacement field becomes:

$$\begin{aligned} u_x &= L_1\, u_{x1} + L_2\, u_{x2} + L_3\, u_{x3} + L_4\, u_{x4} + L_5\, u_{x5} + L_6\, u_{x6} \\ u_y &= L_1\, u_{y1} + L_2\, u_{y2} + L_3\, u_{y3} + L_4\, u_{y4} + L_5\, u_{y5} + L_6\, u_{y6} \\ u_z &= L_1\, u_{z1} + L_2\, u_{z2} + L_3\, u_{z3} + L_4\, u_{z4} + L_5\, u_{z5} + L_6\, u_{z6} \end{aligned} \tag{10}$$

In Figs. 4 the stacking sequences for two linear and parabolic elements are shown. The total amount of variables is related to the order of the expansion as well as the number of elements on the cross-section.

4 FINITE ELEMENT FORMULATION

Finite Element formulation is adopted in order to easily face arbitrary shaped cross-sections. By introducing the shape functions, N_i, and the nodal displacements vector, $\mathbf{q}_{\tau i}$:

$$\mathbf{q}_{\tau i} = \left\{ \begin{array}{ccc} q_{u_{x_{\tau i}}} & q_{u_{y_{\tau i}}} & q_{u_{z_{\tau i}}} \end{array} \right\}^T \tag{11}$$

the displacement vector becomes:

$$\mathbf{u}_\tau = N_i F_\tau \mathbf{q}_{\tau i} \tag{12}$$

For the sake of brevity, the shape functions are not reported here. They can be found in many books, for instance in [18]. Elements with 4 nodes (B4) are formulated. The stiffness matrix of the elements and the external loadings that are consistent to the model are obtained via the Principle of Virtual Displacements:

$$\delta L_{int} = \int_V (\delta \boldsymbol{\epsilon}_p^T \boldsymbol{\sigma}_p + \delta \boldsymbol{\epsilon}_n^T \boldsymbol{\sigma}_n) dV = \delta L_{ext} - \delta L_{ine} \tag{13}$$

where L_{int} stands for the strain energy, L_{int} is the work of the external loadings, and L_{ine} is the work of the inertial loadings. δ stands for the virtual variation. The virtual variation of the strain energy is rewritten using Eq.s 3, 6 and 12, in a compact format it becomes:

$$\delta L_{int} = \delta \mathbf{q}_{\tau i}^T \mathbf{K}^{ij\tau s} \mathbf{q}_{sj} \tag{14}$$

where $\mathbf{K}^{ij\tau s}$ is the stiffness matrix in the form of the fundamental nucleus. Its components are:

$$\begin{aligned}
K_{xx}^{ij\tau s} = {} & \tilde{C}_{11} \int_\Omega F_{\tau,_x} F_{s,_x} d\Omega \int_l N_i N_j dz + \tilde{C}_{16} \int_\Omega F_{\tau,_y} F_{s,_x} d\Omega \int_l N_i N_j dz + \\
& \tilde{C}_{16} \int_\Omega F_{\tau,_x} F_{s,_y} d\Omega \int_l N_i N_j dz + \tilde{C}_{66} \int_\Omega F_{\tau,_x} F_{s,_y} d\Omega \int_l N_i N_j dz + \\
& \tilde{C}_{55} \int_\Omega F_\tau F_s d\Omega \int_l N_{i,_z} N_{j,_z} dz \\
K_{xy}^{ij\tau s} = {} & \tilde{C}_{12} \int_\Omega F_{\tau,_x} F_{s,_y} d\Omega \int_l N_i N_j dz + \tilde{C}_{26} \int_\Omega F_{\tau,_y} F_{s,_y} d\Omega \int_l N_i N_j dz + \\
& \tilde{C}_{16} \int_\Omega F_{\tau,_x} F_{s,_x} d\Omega \int_l N_i N_j dz + \tilde{C}_{66} \int_\Omega F_{\tau,_y} F_{s,_x} d\Omega \int_l N_i N_j dz + \\
& \tilde{C}_{45} \int_\Omega F_\tau F_s d\Omega \int_l N_{i,_z} N_{j,_z} dz \\
K_{xz}^{ij\tau s} = {} & \tilde{C}_{13} \int_\Omega F_{\tau,_x} F_s d\Omega \int_l N_i N_{j,_z} dz + \tilde{C}_{36} \int_\Omega F_{\tau,_y} F_s d\Omega \int_l N_i N_{j,_z} dz + \\
& \tilde{C}_{55} \int_\Omega F_\tau F_{s,_x} d\Omega \int_l N_{i,_z} N_j dz + \tilde{C}_{45} \int_\Omega F_\tau F_{s,_y} d\Omega \int_l N_{i,_z} N_j dz \\
K_{yx}^{ij\tau s} = {} & \tilde{C}_{12} \int_\Omega F_{\tau,_y} F_{s,_x} d\Omega \int_l N_i N_j dz + \tilde{C}_{16} \int_\Omega F_{\tau,_x} F_{s,_x} d\Omega \int_l N_i N_j dz + \\
& \tilde{C}_{26} \int_\Omega F_{\tau,_y} F_{s,_y} d\Omega \int_l N_i N_j dz + \tilde{C}_{66} \int_\Omega F_{\tau,_x} F_{s,_y} d\Omega \int_l N_i N_j dz + \\
& \tilde{C}_{45} \int_\Omega F_\tau F_s d\Omega \int_l N_{i,_z} N_{j,_z} dz \\
K_{yy}^{ij\tau s} = {} & \tilde{C}_{22} \int_\Omega F_{\tau,_y} F_{s,_y} d\Omega \int_l N_i N_j dz + \tilde{C}_{26} \int_\Omega F_{\tau,_x} F_{s,_y} d\Omega \int_l N_i N_j dz + \\
& \tilde{C}_{26} \int_\Omega F_{\tau,_y} F_{s,_x} d\Omega \int_l N_i N_j dz + \tilde{C}_{66} \int_\Omega F_{\tau,_x} F_{s,_x} d\Omega \int_l N_i N_j dz + \\
& \tilde{C}_{44} \int_\Omega F_\tau F_s d\Omega \int_l N_{i,_z} N_{j,_z} dz \\
K_{yz}^{ij\tau s} = {} & \tilde{C}_{23} \int_\Omega F_{\tau,_y} F_s d\Omega \int_l N_i N_{j,_z} dz + \tilde{C}_{36} \int_\Omega F_{\tau,_x} F_s d\Omega \int_l N_i N_{j,_z} dz + \\
& \tilde{C}_{45} \int_\Omega F_\tau F_{s,_x} d\Omega \int_l N_{i,_z} N_j dz + \tilde{C}_{44} \int_\Omega F_\tau F_{s,_y} d\Omega \int_l N_{i,_z} N_j dz \\
K_{zx}^{ij\tau s} = {} & \tilde{C}_{55} \int_\Omega F_{\tau,_x} F_s d\Omega \int_l N_i N_{j,_z} dz + \tilde{C}_{45} \int_\Omega F_{\tau,_y} F_s d\Omega \int_l N_i N_{j,_z} dz + \\
& \tilde{C}_{13} \int_\Omega F_\tau F_{s,_x} d\Omega \int_l N_{i,_z} N_j dz + \tilde{C}_{36} \int_\Omega F_\tau F_{s,_y} d\Omega \int_l N_{i,_z} N_j dz \\
K_{zy}^{ij\tau s} = {} & \tilde{C}_{45} \int_\Omega F_{\tau,_x} F_s d\Omega \int_l N_i N_{j,_z} dz + \tilde{C}_{44} \int_\Omega F_{\tau,_y} F_s d\Omega \int_l N_i N_{j,_z} dz + \\
& \tilde{C}_{23} \int_\Omega F_\tau F_{s,_y} d\Omega \int_l N_{i,_z} N_j dz + \tilde{C}_{36} \int_\Omega F_\tau F_{s,_x} d\Omega \int_l N_{1,_z} N_j dz
\end{aligned} \tag{15}$$

$$K_{zz}^{ij\tau s} = \begin{array}{l} \tilde{C}_{55} \int_\Omega F_{\tau,_x} F_{s,_x} d\Omega \int_l N_i N_j dz + \tilde{C}_{45} \int_\Omega F_{\tau,_y} F_{s,_x} d\Omega \int_l N_i N_j dz + \\ \tilde{C}_{45} \int_\Omega F_{\tau,_x} F_{s,_y} d\Omega \int_l N_i N_j dz + \tilde{C}_{44} \int_\Omega F_{\tau,_y} F_{s,_y} d\Omega \int_l N_i N_j dz + \\ \tilde{C}_{33} \int_\Omega F_\tau F_s d\Omega \int_l N_{i,_z} N_{j,_z} dz \end{array}$$

The virtual variation of the work of the inertial loadings is:

$$\delta L_{ine} = \int_V \rho \ddot{\boldsymbol{u}} \delta \boldsymbol{u}^T dV \tag{16}$$

where ρ stands for the density of the material, and $\ddot{\boldsymbol{u}}$ is the acceleration vector. Eq. 16 is rewritten in a compact manner using Eq.s 3, and 12:

$$\delta L_{ine} = \delta \mathbf{q}_{\tau i}^T \mathbf{M}^{ij\tau s} \ddot{\boldsymbol{q}}_{sj} \tag{17}$$

where $\ddot{\boldsymbol{q}}$ is the nodal acceleration vector. $\mathbf{M}^{ij\tau s}$ is the mass matrix in the form of the fundamental nucleus. Its components are:

$$\begin{array}{c} M_{xx}^{ij\tau s} = M_{yy}^{ij\tau s} = M_{zz}^{ij\tau s} = \rho \int_\Omega F_\tau F_s d\Omega \int_l N_i N_j dz \\ M_{xy}^{ij\tau s} = M_{xz}^{ij\tau s} = M_{yx}^{ij\tau s} = M_{yz}^{ij\tau s} = M_{zx}^{ij\tau s} = M_{zy}^{ij\tau s} = 0 \end{array} \tag{18}$$

It should be noted that no assumptions on the approximation order have been done. It is therefore possible to obtain refined beam models without changing the formal expression of the nucleus components.
The loadings vector variationally consistent to the model is derived for the case of a generic concentrated load **P**:

$$\mathbf{P} = \left\{ \begin{array}{ccc} P_{u_x} & P_{u_y} & P_{u_z} \end{array} \right\}^T \tag{19}$$

Any other loading condition can be similarly treated. The virtual work due to **P** is:

$$\delta L_{ext} = \mathbf{P} \delta \mathbf{u}^T \tag{20}$$

By substituting Eq. (12), the previous equation becomes:

$$\delta L_{ext} = F_\tau N_i \mathbf{P} \delta \mathbf{q}_{\tau i}^T \tag{21}$$

This last equation permits the identification of the components of the nucleus which have to be loaded. In case of first order expansion and **P** acting along x direction only, the virtual external work is:

$$\delta L_{ext} = P_{u_x} \, L_1(x_p, y_p) \, \delta u_{x1} + P_{u_x} \, L_2(x_p, y_p) \, \delta u_{x2} + P_{u_x} \, L_3(x_p, y_p) \, \delta u_{x3} + P_{u_x} \, L_4(x_p, y_p) \, \delta u_{x4} \tag{22}$$

where $[x_p, \ y_p]$ are the coordinate on the cross-section of the loading application point.
The undamped dynamic problem can be written as it follows:

$$\boldsymbol{M} \ddot{\boldsymbol{a}} + \boldsymbol{K} \boldsymbol{a} = \boldsymbol{p} \tag{23}$$

where $\boldsymbol{a}$ is the vector of the nodal unknowns and **p** is the loadings vector. Introducing harmonic solutions, it is possible to compute the natural frequencies, ω_k, for the homogenous case, by solving an eigenvalues problem:

$$(-\omega_k^2 \mathbf{M} + \mathbf{K}) \boldsymbol{a}_k = 0 \tag{24}$$

where $\boldsymbol{a}_k$ is the k-th eigenvector.

5 RESULTS AND DISCUSSION

Static and free vibrations responses of different beam models are investigated. Clamped and simply supported boundary conditions are accounted for. Beams are supposed to have square cross-section. The coordinate frame and the cross-section geometry are shown in Figs. 1 and 2. The thickness of the section, h, is equal to 0.2 [m]. The span-to-height ratio, L/h, is equal to 100. An isotropic material is used. The Young's modulus, E, is equal to 75 [GPa]. The Poisson ratio, ν, is equal to 0.33.

5.1 BENDING

The bending analysis is conducted on a cantilever beam undergoing a vertical force, P_{u_y}, equal to -50 [N]. The loading is applied at the tip cross-section. The mechanics of the beam is described in terms of the maximum vertical displacement, u_y, which is computed at the tip cross-section. A reference solution is obtained according to the following formula:

$$u_{y_b} = \frac{P_{u_y} L^3}{3EI} \tag{25}$$

where I is the moment of inertia of the cross-section.
Table 1 shows the free tip displacement for different mesh along z direction and different cross-section kinematics model. B4 elements are used. Five finite element models are considered: Euler Bernoulli (EBBM), Timoshenko (TBM), a fourth order Taylor-type expansion (N = 4), linear as well parabolic Lagrange polynomials (Q4 and Q9, respectively). EBBM, TBM and fourth order model show a fast convergence behavior since a slender beam loaded at the free tip is considered. Linear Lagrange polynomials are affected by poor convergence rate, while Q9 model is able to detect the solution by using 40 beam elements along z axis. In Table 2 a convergence study on the number of Q4 and Q9 elements is conducted. Increasing the number of linear elements improves the solution. No effects are observed as multiple Q9 elements are exploited. Fig. 5 shows the results obtained through different combinations of longitudinal (B2, B3 and B4) and cross-section elements (Q4 and Q9). The usage of linear elements has a detrimental effect on the solution. The combined use of Q9 and B3 or B4 permits to yield the benchmark value.

5.2 TRACTION

As second assessment, a cantilever beam undergoing a traction force, P_{u_z}, equal to 50 [N], is considered. The loading is applied at the tip cross-section.The mechanics of the beam is described in terms of axial displacement, u_z, which is computed at the tip cross-section. A reference solution is obtained according to the following formula:

$$u_{z_b} = \frac{P_{u_z} L}{EA} \tag{26}$$

where A is the cross-section area.
Table 3 reports the results obtained through different Lagrange expansions using B4 elements. Linear elements match the benchmark results with no need of further refinements. In Fig. 6 different combinations of elements are addressed. B2 elements show considerably poorer convergence rate than B3 and B4 both with Q4 and Q9.

5.3 FREE VIBRATIONS

For dynamics analysis the beam is modeled as simply supported. The first four bending modes are analyzed. As benchmark for the k-th natural frequency, Euler-Bernoulli solution [19] is used:

$$f_{k_b} = \frac{\pi}{2}\left(\frac{k}{L}\right)^2\left(\frac{EI}{\rho A}\right)^{\frac{1}{2}} \tag{27}$$

Table 4 shows the first four natural frequencies for different beam theories. They are related to bending modes .Parabolic Lagrange polynomials are able to match the benchmark values. Q4 elements furnishes higher frequencies, that is, they overestimate the stiffness of the structure.

6 CONCLUSIONS

Refined beam theories with only displacement degrees of freedom based on Carrera Unified Formulation have been presented in this work. Lagrange polynomials have been exploited to describe the cross-section kinematics field. Finite element analysis has been implemented for the structural investigation of beams with different layouts. Static as well as free-vibrations analysis have been faced. The obtained results have been compared with classical theories and Taylor-type fourth order models.
It is mainly concluded that:

- the proposed model is able to detect correct results;
- CUF permits to deal with arbitrary higher order models with no need of *ad hoc* implementations;

Parabolic polynomials or multiple linear cross-section elements have to be preferred to obtain sufficiently accurate results. Lagrange elements offer a wide range of applications that will be developed in future works:

- analysis of multilayered beams via layer-wise formulation;
- implementation of non-linear structural analysis;
- extensions to aeroelastic problems.

References

[1] K. Kapania and S. Raciti. Recent advances in analysis of laminated beams and plates, part I: Shear effects and buckling. *AIAA JOURNAL*, 27(7):923-935, 1989.

[2] K. Kapania and S. Raciti. Recent advances in analysis of laminated beams and plates, part II: Vibrations and wave propagation. *AIAA JOURNAL*, 27(7):935-946, 1989.

[3] C. Kim and S. R. White. Thick-walled composite beam theory including 3-D elastic effects and torsional warping. *International Journal of Solid Structures*, 34(31-32):4237-4259, 1997.

[4] J. N. Reddy. On locking-free shear deformable beam finite elements. *Computer methods in applied mechanics and engineerlng*, 149:113-132, 1997.

[5] G. Shi and K. Y. Lam. Finite element vibration analysis of composite beams based on higher-order beam theory. *Journal of Sound and Vibration*, 219(4):707721, 1999.

[6] J. Lee. Flexural analysis of thin-walled composite beams using shear-deformable beam theory. *Composite Structures*, 70(2):212-222, 2005.

[7] A. L. Gol'denweizer. Derivation of an approximate theory of bending of a plate by the method of asymptotic integration of the equations of the theory of elasticity. *Prikl. Mat. Mekh.*, 26:1000-1025, 1962.

[8] A. L. Gol'denweizer. Derivation of an approximate theory of shells by means of asymptotic integration of the equations of the theory of elasticity. *Prikl. Mat. Mekh.*, 27:903-924, 1963.

[9] P. Cicala. Systematic approximation approach to linear shell theory. *Levrotto e Bella*, Torino, 1965.

[10] V. V. Volovoi, D. H. Hodges, V. L. Berdichevsky, and V. G. Sutyrin. Asymptotic theory for static behavior of elastic anisotropic I-beams. *International Journal of Solid Structures*, 36:1017-1043, 1999.

[11] V. V. Volovoi and D. H. Hodges. Theory of anisotropic thin-walled beams. *Journal of Applied Mechanics*, 67:453-459, 2000.

[12] W. Yu, V. V. Volovoi, D. H. Hodges, and X. Hong. Validation of the variational asymptotic beam sectional analysis (VABS). *AIAA Journal*, 40:2105-2113, 2002.

[13] G. Giunta, E. Carrera, and S. Belouettar. A refined beam theory with only displacement variables and deformable cross-section. *50th AIAA/ASME/ASCE/AHS/ASC Structures, Structural Dynamics, and Materials Conference, Palm Springs, California 4 - 7 May 2009*. 2009.

[14] S. W. Tsai. *Composites Design*. Dayton, Think Composites, 4th edition, 1988.

[15] J. N. Reddy. *Mechanics of laminated composite plates and shells. Theory and Analysis*. CRC Press, 2^{nd} edition, 2004.

[16] E. Carrera. Theories and finite elements for multilayered plates and shells. *Archives of Computational Methods in Engineering*, 9(2):87140, 2002.

[17] E. Carrera and G. Giunta. Refined beam theories based on Carrera's unified formulation. Submitted.

[18] K.J. Bathe. *Finite element procedure*. Prentice hall, 1996.

[19] R. R. Craig Jr. *Structural dynamics*. John Wiley and Sons, 1981.

No. Elem.	EBBM	TBM	$N = 4$	Q4	Q9
$u_y \times 10^2$ [m], $u_{y_b} \times 10^2 = -1.333$ [m], B4					
3	-1.334	-1.334	-1.334	-0.565	-1.296
5	-1.334	-1.334	-1.334	-0.778	-1.311
10	-1.334	-1.334	-1.334	-0.945	-1.323
40	-1.334	-1.334	-1.334	-1.073	-1.331

Table 1: Maximum vertical displacement for different beam models and number of elements. Loading case: bending.

No. Elem.	$1\times$ Q4	$2\times$ Q4	$3\times$ Q4	$4\times$ Q4	$1\times$ Q9	$2\times$ Q9
$u_y \times 10^2$ [m], $u_{y_b} \times 10^2 = -1.333$ [m], B4						
3	-0.565	-1.209	-1.237	-1.249	-1.296	-1.296
5	-0.778	-1.220	-1.250	-1.262	-1.311	-1.311
10	-0.945	-1.228	-1.259	-1.271	-1.323	-1.323
40	-1.073	-1.234	-1.265	-1.278	-1.331	-1.331

Table 2: Maximum vertical displacement for different cross-section kinematics models. Loading case: bending.

No. Elem.	$1\times$ Q4	$2\times$ Q4	$3\times$ Q4	$4\times$ Q4	$1\times$ Q9	$2\times$ Q9
$u_z \times 10^7$ [m], $u_{z_b} \times 10^7 = 3.333$ [m], B4						
3	3.307	3.307	3.307	3.306	3.309	3.307
5	3.317	3.317	3.317	3.316	3.321	3.317
10	3.325	3.325	3.325	3.323	3.332	3.325
40	3.331	3.331	3.331	3.325	3.352	3.331

Table 3: Free tip axial displacement for different cross-section kinematics models. Loading case: traction.

[Hz]	Re. Sol. Eq. 27	EBBM	TBM	$N = 4$	Q4	Q9
f_1	1.195	1.195	1.194	1.194	1.306	1.194
f_2	4.780	4.778	4.775	4.775	5.221	4.777
f_3	10.755	10.747	10.737	10.735	11.736	10.740
f_4	19.119	19.102	19.068	19.064	20.840	19.074

Table 4: First four bending frequencies of the simply supported beam for different kinematics models.

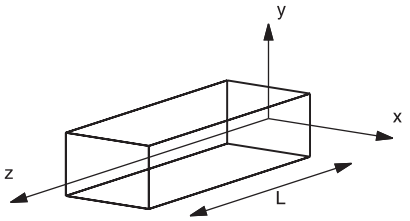

Figure 1: Coordinate frame and geometry of a rectangular beam.

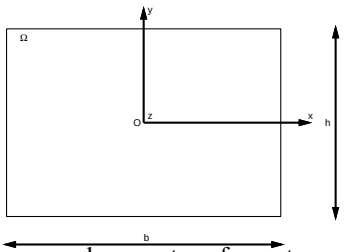

Figure 2: Coordinate frame and geometry of a rectangular cross-section.

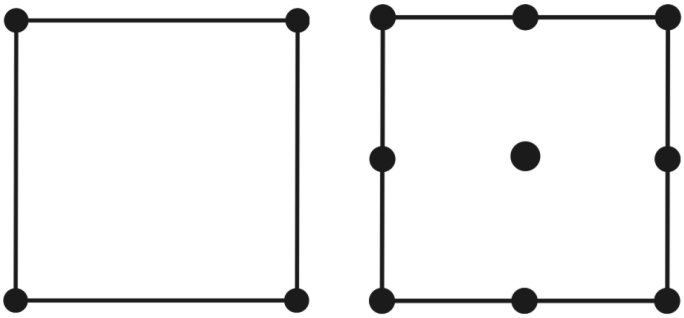

(a) Q4 (b) Q9

Figure 3: Sampling points locations within the cross-section.

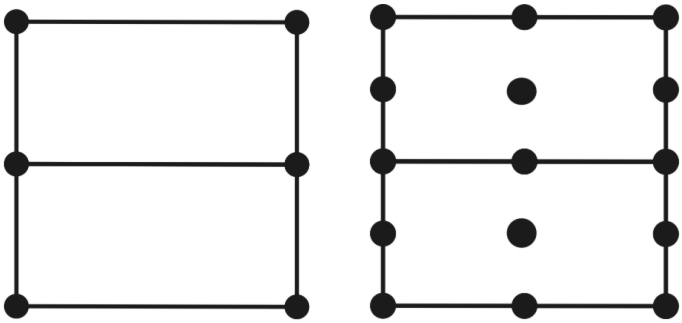

(a) 2× Q4 (b) 2× Q9

Figure 4: Examples of assembling of stacked Lagrange elements.

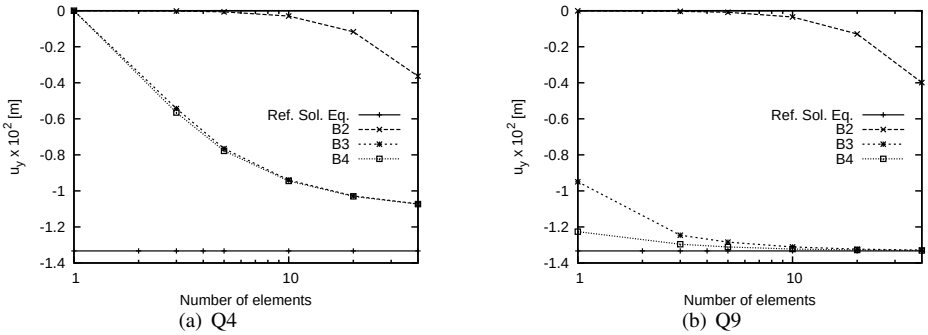

(a) Q4 (b) Q9

Figure 5: Convergence behavior for Q4 and Q9 elements. Loading Case: bending.

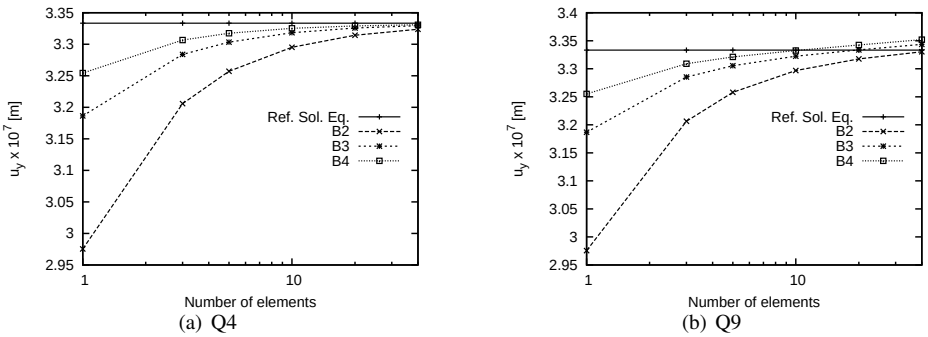

(a) Q4 (b) Q9

Figure 6: Convergence behavior for Q4 and Q9 elements. Loading case: traction.